Numerical method for the calculation of continuum excitation amplitudes in time-dependent external field problems

C. Bottcher and M. R. Strayer
Physics Division, Oak Ridge National Laboratory, Oak Ridge, Tennessee 37831

A. S. Umar and V. E. Oberacker
Department of Physics and Astronomy, Vanderbilt University, Nashville, Tennessee 37235

(Received 11 January 1988)

We introduce a new numerical method for calculating continuum excitation probabilities of complex physical systems under the influence of external, time-dependent, and nonperturbative fields. The method utilizes a discretized form of the Hamiltonian on a space lattice and is particularly suited for large scale computations involving many-body systems. We perform a comparative study for a model problem by solving the same time-dependent Schrödinger equation in spherical and cylindrical coordinates. As a realistic example, we apply the method to the problem of prompt nucleon emission in low energy heavy-ion reactions.

I. INTRODUCTION

A large class of problems in nuclear and atomic physics involves the excitation of continuum states by a time-dependent external field acting on a complex many-body system. Processes such as the prompt nucleon emission in heavy-ion reactions[1] or electrons ejected in ion-atom and atom-atom collisions[2] convey information about the details of the collision dynamics. While the data are commonly interpreted in terms of classical methods or the Born approximation, more satisfactory approaches incorporate the dynamical evolution of the collision process. Examples of dynamical formalisms include the semiclassical description of nuclear[1] and atomic collisions.[3,4] Continuum excitation problems also occur in nonperturbative quantum field theories,[5] e.g., lepton-pair production in relativistic heavy-ion reactions[6] and inclusive γ and π^0 production in intermediate and high-energy heavy-ion reactions.[7,8] Although we will confine ourselves in this paper to nonrelativistic problems, the method is readily applicable to relativistic systems.

The calculation of continuum excitation requires the knowledge of both bound and continuum states for the system. In general, the computation of scattering states for a many-body system is far more difficult than the calculation of bound states. In most practical calculations, the Hamiltonian is represented numerically on a discrete mesh. In principle, the continuum excitation problem can be studied by diagonalizing the resulting finite Hamiltonian matrix, which yields a fixed number of bound states and discretized continuum states with standing wave boundary conditions. Projection of the time-evolved states onto the continuum states, followed by an averaging of the discrete amplitudes over a finite energy interval, gives the desired approximation to the continuum excitation spectrum. However, this straightforward approach gives rise to serious problems:

(a) For a realistic two- or three-dimensional calculation, the size of the matrix to be diagonalized is prohibitively large.

(b) Other methods for the calculation of scattering states such as the solution of the Lippmann-Schwinger scattering equation,[9] and the R-matrix approach[10] are also impaired by the requirement of a small Hamiltonian matrix. Due to numerical inaccuracy, the calculated scattering states are no longer orthogonal to the bound states and they do not satisfy the Schrödinger equation. Accurate numerical computations are only possible under very special circumstances, for example when the potential can be written in a separable form,[11,12] or when it is naturally given in terms of basis functions of Slater's type.[13]

Therefore, it is highly desirable to develop a formalism which makes effective use of the discretized Hamiltonian to calculate the continuum transition amplitudes for complex systems. In our formalism, the Hamiltonian matrix is never explicitly stored. Rather, it is known implicitly through its action on the state vectors, thus making the problem tractable. In Sec. II we introduce the formalism. In Sec. III this formalism is applied to a model problem, and in Sec. IV to the problem of prompt nucleon emission in low energy heavy-ion reactions.

II. FORMALISM

Let us consider an isolated many-body system which is described by the free Hamiltonian H_0; the kets $|\phi_\alpha\rangle$ and $|\phi_{\mathbf{k}}\rangle$ denote the bound states and exact continuum eigenstates, with standing wave boundary conditions, respectively

$$\begin{aligned} &H_0|\phi_\alpha\rangle=\epsilon_\alpha|\phi_\alpha\rangle, \quad \alpha=1,\ldots,A \ , \\ &H_0|\phi_{\mathbf{k}}\rangle=\epsilon_k|\phi_{\mathbf{k}}\rangle \ . \end{aligned} \tag{1}$$

During the time interval $-T<t<+T$, the system is subjected to an external time-dependent potential $V(t)$. The time evolution of the system is given by the state vector $|\psi_\alpha(t)\rangle$ which is determined by the time-dependent

Schrödinger equation

$$H(t)\,|\,\psi_\alpha(t)\rangle=[H_0+V(t)]\,|\,\psi_\alpha(t)\rangle=i\hbar\frac{\partial}{\partial t}\,|\,\psi_\alpha(t)\rangle\ , \tag{2}$$

subject to the conditions

$$\lim_{|t|\to\infty} H(t)=H_0\ ,$$

$$\lim_{t\to-\infty}\,|\,\psi_\alpha(t)\rangle=e^{-i\epsilon_\alpha t/\hbar}\,|\,\phi_\alpha\rangle\ . \tag{3}$$

Consider the operator

$$F(E)=\left[\frac{1}{\sqrt{\pi}\Delta}\right]^{1/2} e^{-(H_0-E)^2/2\Delta^2}\ , \tag{4}$$

where, in practice, H_0 is an operator acting on state vectors, and Δ is a parameter which will be discussed shortly. Using $F(E)$, we form the new ket

$$|\,\chi_\alpha(E)\rangle=F(E)\,|\,\psi_\alpha(T)\rangle\ , \tag{5}$$

which is normalized to unity

$$\int_{-\infty}^{+\infty} dE\,\langle\chi_\alpha(E)\,|\,\chi_\alpha(E)\rangle=1\ , \tag{6}$$

as can easily be seen by expanding $|\,\psi_\alpha(t)\rangle$ in terms of the complete set of states of H_0. The following overlap

$$f_\alpha(E)=\langle\chi_\alpha(E)\,|\,\chi_\alpha(E)\rangle \tag{7}$$

can be used to extract the differential excitation probability. To this end, we insert a complete set of eigenstates of H_0 into Eq. (7)

$$f_\alpha(E)=\sum_\lambda \langle\psi_\alpha(T)\,|\,F^\dagger(E)\,|\,\phi_\lambda\rangle\langle\phi_\lambda\,|\,F(E)\,|\,\psi_\alpha(T)\rangle$$

$$=f_\alpha^B(E)+f_\alpha^C(E)\ , \tag{8}$$

where f_α^B and f_α^C denote the bound and continuum state contributions to the summation, respectively

$$f_\alpha^B(E)=\frac{1}{\sqrt{\pi}\Delta}\sum_{\beta=1}^{A}\,|\,\langle\psi_\alpha(T)\,|\,\phi_\beta\rangle\,|^2 e^{-(\epsilon_\beta-E)^2/\Delta^2}\ ,$$

$$f_\alpha^C(E)=\frac{1}{\sqrt{\pi}\Delta}\int\frac{d^3k}{(2\pi)^3}\,|\,\langle\psi_\alpha(T)\,|\,\phi_{\mathbf{k}}\rangle\,|^2 e^{-(\epsilon_k-E)^2/\Delta^2}\ . \tag{9}$$

After a change of variables, the quantity f_α^C can be written as

$$f_\alpha^C(E)=\frac{1}{\sqrt{\pi}\Delta}\int_0^\infty d\epsilon_k C_\alpha(\epsilon_k) e^{-(\epsilon_k-E)^2/\Delta^2}\ , \tag{10}$$

where

$$C_\alpha(\epsilon_k)=\frac{1}{2}\left[\frac{2m}{\hbar^2}\right]^{3/2}\frac{\sqrt{\epsilon_k}}{(2\pi)^3}\int\,|\,\langle\psi_\alpha(T)\,|\,\phi_{\mathbf{k}}\rangle\,|^2 d\Omega_k\ . \tag{11}$$

We see from Eqs. (9)–(11) that the quantity C_α is the angle-integrated differential excitation probability for state α

$$\frac{dP_\alpha(\epsilon_k)}{d\epsilon_k}=C_\alpha(\epsilon_k)\ , \tag{12}$$

and it can be used to calculate differential and total cross sections.[1]

The left-hand side of Eq. (8) can be computed numerically. In evaluating the action of $F(E)$ on the ket $|\,\psi_\alpha(T)\rangle$ in Eq. (5) we use the power series expansion of the exponential operator. However, a direct expansion of the exponential gives nonconvergent results for a reasonable number of terms. This problem can be circumvented by making use of the operator identity

$$e^A=[e^{A/N}]^N\ , \tag{13}$$

which yields from Eqs. (5), (7), and (8)

$$f_\alpha^C(E)=\frac{1}{\sqrt{\pi}\Delta}\langle\psi_\alpha(T)\,|\,[e^{-(H_0-E)^2/(\Delta^2 N)}]^N\,|\,\psi_\alpha(T)\rangle$$

$$-f_\alpha^B(E)\ . \tag{14}$$

Here, the value of N is adjusted to ensure the convergence of the exponential series, in addition to the convergence of the entire operator. This series can be generated by repeated operations of (H_0-E) on $|\,\psi_\alpha(T)\rangle$. This procedure was used to obtain convergence to 1 part in 10^7 or better. The quantity f_α^B can be computed directly from (9), since we have full knowledge of the bound and time evolved states. Consequently, Eq. (14) enables us to calculate $f_\alpha^C(E)$ which allows the extraction of the differential excitation probability via a deconvolution of the Gaussian integral in Eq. (10). This deconvolution is most easily done by assuming a parametric form for $C_\alpha(\epsilon)$ and adjusting the parameters to obtain the desired equality. The full amplitude could be similarly obtained by making a deconvolution in both energy and angle. Here, the Gaussian operator acts as a smoothing or averaging tool over an energy interval Δ. For this reason the value of Δ should be chosen to cover an energy range which includes a reasonable number of continuum states. This is tested numerically by changing the value of Δ and looking for convergence. However, we should keep in mind that in a discrete approximation to the continuum spectrum the spacing between states increases with increasing energy. Therefore, beyond a certain energy the results may become unreliable. In two- and three-dimensional calculations the large number of states ensures that this limit is very high. Another consideration in the choice of Δ is the widths of the possible structures in the excitation functions. In such a case, the size of the parameter Δ should be comparable to the width of the structures, otherwise a smoothing of the structures will take place.

III. A MODEL CALCULATION

The numerical formalism described in the previous section can be most reliably applied to problems in two- and three-dimensions where the density of continuum states is large and therefore an accurate calculation of Eq. (14) is feasible. Consequently, it is difficult to find realistic problems that can also be solved analytically. In order to be

able to perform a realistic comparison with a soluble problem, we study the time-dependent Schrödinger equation using spherically symmetric static and time-dependent potentials with two different approaches:

(a) We make a partial wave decomposition of the Schrödinger equation and solve the resulting time-independent and time-dependent radial equations. Since the radial equation is essentially a one-dimensional problem, the calculation of the continuum transition amplitudes can be done by direct diagonalization of the discrete Hamiltonian.

(b) In the second approach we solve the same set of equations in cylindrical polar coordinates and calculate the excitation probability via Eq. (14). Furthermore, we repeat the radial calculation using a very large one-dimensional box which has a reasonable number of low energy continuum states and allows us yet another way to calculate Eq. (14).

We choose the static potential parameters such that there is only one bound s-wave state which we then time evolve using an external potential, thus preserving the spherical symmetry. Of course the comparison of the excitation probabilities, calculated in (a) and (b), will be limited by the intrinsic numerical differences arising from the employment of radically different numerical procedures in the two calculations. We now proceed to describe the numerical solutions of the steps (a) and (b).

Consider the time-dependent Schrödinger equation for a particle of mass m

$$\left[-\frac{\hbar^2}{2m}\nabla^2+V+W(t)\right]|\psi_\alpha(t)\rangle=i\hbar|\dot{\psi}_\alpha(t)\rangle\ , \tag{15}$$

where the static and time-dependent potentials V and W are local potentials given by,

$$\begin{aligned} V(\mathbf{r})&=V_0e^{-r^2/a^2}\ ,\\ W(\mathbf{r},t)&=W_0e^{-r^2/r_s^2}e^{-t^2/\tau^2}\ . \end{aligned} \tag{16}$$

In the asymptotic past ($t\rightarrow-\infty$) Eqs. (1) and (3) are satisfied.

In case (a) we make a partial-wave decomposition of Eq. (15) obtaining the radial Schrödinger equation (s wave)

$$\left[-\frac{\hbar^2}{2m}\frac{d^2}{dr^2}+V\right]|\chi_\alpha\rangle=\epsilon_\alpha|\chi_\alpha\rangle\ , \tag{17}$$

where

$$\chi_\alpha(r)=r\phi_\alpha(r)\ , \tag{18}$$

and r denotes the radial coordinate. This equation is then discretized on a coordinate mesh

$$r_i=i\Delta r,\quad i=1,\ldots,N_r,\quad \chi_{\alpha,i}\equiv\chi_\alpha(r_i)\ , \tag{19}$$

using the three-point finite-difference approximation for the second derivative

$$-\frac{\hbar^2}{2m(\Delta r)^2}(\chi_{\alpha,i+1}-2\chi_{\alpha,i}+\chi_{\alpha,i-1})+V_i\chi_{\alpha,i}=\epsilon_\alpha\chi_{\alpha,i}\ , \tag{20}$$

subject to the boundary conditions

$$\chi_{\alpha,0}=0=\chi_{\alpha,N+1}\ . \tag{21}$$

Equation (20) can be written as a matrix problem

$$H_0\cdot\begin{bmatrix}\chi_{\alpha,1}\\ \chi_{\alpha,2}\\ \vdots\\ \chi_{\alpha,N}\end{bmatrix}=\epsilon_\alpha\begin{bmatrix}\chi_{\alpha,1}\\ \chi_{\alpha,2}\\ \vdots\\ \chi_{\alpha,N}\end{bmatrix}\ , \tag{22}$$

with

$$H_0=\begin{bmatrix} a_1 & b & \cdots & & & \\ b & a_2 & b & \cdots & & \\ 0 & b & a_3 & b & \cdots & \\ & \ddots & \ddots & \ddots & & \\ & & & & & b \\ & & & & b & a_N \end{bmatrix}\ . \tag{23}$$

The elements of H_0 are given by

$$\begin{aligned} a_i&=\frac{\hbar^2}{m(\Delta r)^2}+V_i\ ,\\ b&=-\frac{\hbar^2}{2m(\Delta r)^2}\ . \end{aligned}$$

Diagonalization of H_0 gives N_r eigenvalues and the corresponding eigenvectors evaluated at the mesh points. The bound state (for simplicity we choose the potential parameters to have a single bound state) is then evolved in discrete time steps $t_n=n\Delta t$ using the Crank-Nicholson approximation to the propagator[14]

$$\begin{aligned} |\psi_b(t_n+\Delta t)\rangle=&\left[1+i\frac{\Delta t}{2\hbar}H^{n+1/2}\right]^{-1}\\ &\times\left[1-i\frac{\Delta t}{2\hbar}H^{n+1/2}\right]|\psi_b(t_n)\rangle\ , \end{aligned} \tag{24}$$

where $H^{n+1/2}$ is the half-time-step Hamiltonian,

$$H^{n+1/2}=-\frac{\hbar^2}{2m}\frac{d^2}{dr^2}+V+W\left[t_n+\frac{\Delta t}{2}\right]\ . \tag{25}$$

In practical calculations we have used the following values for the potential parameters for both (a) and (b)

$$\begin{aligned} &V_0=-20\ \text{MeV}\ ,\\ &a=3\ \text{fm}\ ,\\ &W_0=50\ \text{MeV}\ ,\\ &r_s=5\ \text{fm}\ ,\\ &\tau=10\ \text{fm}/c\ . \end{aligned}$$

With these values of V_0 and a the potential has a single bound s wave with an energy $\epsilon_b=-4.346\,32$ MeV. The parameters of the time dependent, external potential, W_0, r_s, and τ are chosen to give a substantial total continuum transition probability. For the solution of the radial

equation we have used the following space-time lattice parameters

$$N_r = 1400 ,$$

$$\Delta r = 0.1 \text{ fm} ,$$

$$N_t = 1400 ,$$

$$\Delta t = 0.05 \text{ fm}/c .$$

The choice of a large box size compresses the discrete continuum spectrum giving us 97 states between 0 and 100 MeV. In Fig. 1 we observe the time development of the total excitation probability

$$P(t) = 1 - |\langle \psi_b(t) | \chi_b \rangle|^2 . \tag{26}$$

Notice that we have a substantial probability for continuum excitations, and $P(t)$ approaches the constant value $P(t=\infty) = 0.523\,47$. The projection of the time evolved state onto the positive energy eigenstates of H_0 yields the quantity dP/dn where n denotes a discrete eigenfunction index. However, this quantity does not contain the appropriate energy weights which is the case for all matrix diagonalizations. The quantity dP/dn should be multiplied by the density of states $dn/d\epsilon$ to give $dP/d\epsilon$. This can be done approximately by using the Stieltjes method which has been extensively used in the study of photoionization and electron impact collisions.[15]

$$\frac{dP}{d\epsilon}\left[\frac{\epsilon_n + \epsilon_{n+1}}{2}\right] = \left[\frac{P_n + P_{n+1}}{2}\right]\left[\frac{1}{\epsilon_{n+1} - \epsilon_n}\right] . \tag{27}$$

This expression is exact when the number of states becomes infinite.

In the second part of the study, we solve the static and time-dependent Schrödinger equations in cylindrical polar coordinates using the same potentials as in the case (a). For the numerical representation of these equations, we use the "variation on the mesh" method,[16] which is described in Appendix A. This method yields a stable numerical algorithm for the solution of such large scale problems and does not require the storage of large matrices since we only use the action of the Hamiltonian on the state vectors. For the calculation of the bound state, we used the gradient-iteration method as described in Appendix A. For mesh values $N_r = 100$, $N_z = 160$, and $\Delta r = \Delta z = 0.2$ fm, the agreement between the lowest s wave eigenvalues of the two calculations is 0.2%. For the time-evolution we have used the Peaceman-Rachford method (see Appendix A for details) and the same N_t and Δt as in the solution of the radial equation. The total integrated continuum excitation probability differed from the spherical case by approximately 0.3%. In view of the rather drastic differences between the numerical methods used to solve the spherical and cylindrical problems, these results are impressively accurate. However, we also note that the difference between the two methods will be reflected in our comparison of the excitation spectra.

We next calculate the excitation spectra for the cylindrical problem using the method described in Sec. I, Eq. (14). This is accomplished by a 25 term series expansion of the exponential operator which is generated by repeated applications of $(H_0 - E)$ on the state vector. For a given E and Δ, the desired convergence (1 part in 10^7) is achieved by choosing a large enough value for power N. The value of N is closely related to the change in the energy averaging parameter Δ. This quantity approximately satisfies the equation $N\Delta^2 = constant$. The constant can be determined by making a quick run with a large Δ which requires a small value for N. Consequently, for a given Δ the value of N can be estimated quite accurately. In Fig. 2 we plot the quantity $f(E)$ of Eq. (6) as a function of E and for various values of Δ. Of course, this is still convoluted with the Gaussian operator. The decon-

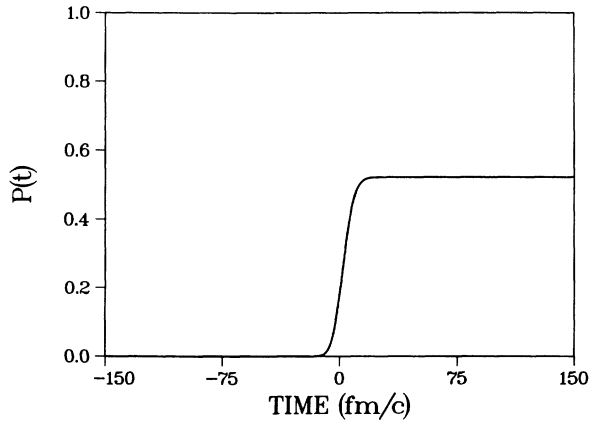

FIG. 1. Time development of the continuum excitation probability $P(t)$ as a function of time (fm/c) for the model problem studied in Sec. III.

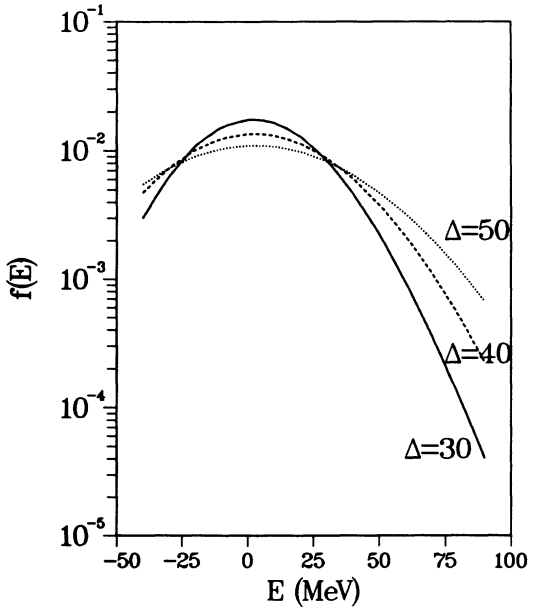

FIG. 2. The quantity $f(E)$ of Eq. (8) as a function of the auxiliary energy E (MeV) for various values of Δ. Deconvolution of this quantity (after the subtraction of the bound state contribution) yields the continuum excitation functions.

volution is done by assuming an analytic form for the excitation spectrum

$$\frac{dP}{d\epsilon_k} = K\sqrt{\epsilon_k}\, e^{-\epsilon_k/T} . \tag{28}$$

Here, K and T are parameters determined by a nonlinear least-squares fit to satisfy the equality in Eq. (8) [recall that $f^C(E)$ is obtained by subtracting the bound state contribution from $f(E)$]. In Fig. 3 we plot the excitation probabilities obtained by the two methods. As we see, the curves agree quite well in general with small exceptions. The discrepancy between the two curves is due to the different numerical methods used in the one- and two-dimensional calculations, and to the approximate nature of the Stiltjes imaging method used in the radial problem. Consequently, the small disagreement between the two calculations should not be interpreted as the accuracy limit of the formalism. The Δ values used in these calculations were 30, 40, and 50 MeV. The corresponding N values were 900, 500, and 300, respectively. The curves for all these Δ values overlie one another and the differences will not be observable on Fig. 3. We have also repeated the above calculations for the large one-dimensional box. We find that the radial projection results are in agreement with the cylindrical ones to within two significant digits. However, the value of N required for the convergence of the exponential operator was about 3500 for $\Delta = 30$ MeV. This implies that the numerical work required for the projection remains approximately constant as we increase the dimensionality of the problem.

IV. PROMPT NUCLEON EMISSION

We have also applied the method to the problem of prompt nucleon emission in low energy heavy-ion collisions. Here, the experimental differential singles yield $dN/d\epsilon$ is characterized by a Lorentzian energy distribution. In the mean-field theory of prompt nucleon emission,[1] the classical limit for the relative motion of the two nuclei is taken. Consequently, the full many-body problem is reduced to an external field, generated by one ion, acting on the emitting nucleus. The emitting nucleus is represented by a determinantal wave function in the Hartree-Fock (HF) approximation. The model was previously tested by using a separable, phenomenological interaction which simplified the numerical computation of the continuum states.

Here, we solve the time-dependent Schrödinger equation, with $H_0 = H_{\rm HF}$, on an axially symmetric spatial grid with mesh spacings $\Delta r = \Delta z = 0.25$ fm and number of mesh points $N_r = 25$, $N_z = 50$, using the numerical methods described in Ref. 16, the Skyrme force, and a time step of $\Delta t = 0.4$ fm/c. The ions approach each other on a classical Coulomb trajectory. The problem is formulated in a rotating frame in which the internuclear distance vector is always directed along the z axis, $\mathbf{R}(t) = Z(t)\hat{e}_z$. The external nuclear field has the form

$$V[r,z;Z(t)] = V_0 \frac{1}{1+e^{(x-r_s)/a}}, \quad x^2 = r^2 + [z - Z(t)]^2 . \tag{29}$$

The strength V_0 and range r_s of the nuclear potential are

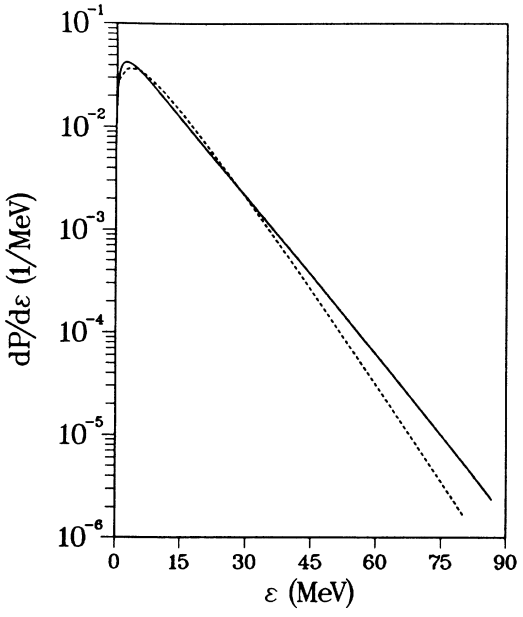

FIG. 3. The continuum excitation function, $dP/d\epsilon$ (1/MeV), as a function of excitation energy (MeV). The solid curve is the result of the spherical calculation, whereas the dashed curve corresponds to the cylindrical calculation and using the projection method discussed in this paper.

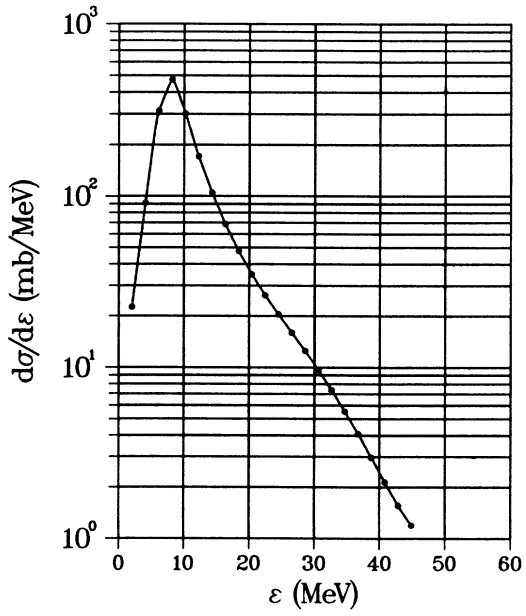

FIG. 4. Energy spectrum $d\sigma/d\epsilon$ (mb/MeV) of prompt nucleons emitted in the deep-inelastic reaction $^{16}O + {}^{93}Nb$, using the new projection method discussed here.

calculated self-consistently by a folding procedure which utilizes the empirical values of the total volume integral and the radius of the nucleon-nucleon potential.[17] The numerical computations were performed to study neutron emission in the deep-inelastic reactions $^{16}O+^{93}Nb$ at $E_{lab}=204$ MeV. For this system, $V_0=60.5$ MeV, $r_s=5.1$ fm, and $a=0.8$ fm. Our calculated total neutron emission multiplicity is within the experimental uncertainty.[18] The value of Δ for the numerical projection was determined to be 20 MeV. The exponent N in Eq. (14) was about 1700 to give the desired numerical accuracy. Figure 4 shows the differential cross section (in the laboratory frame) obtained from

$$\frac{d\sigma}{d\epsilon}=2\pi\sum_{\alpha=1}^{A} n_\alpha \int_{b_{\min}}^{b_{\max}} db\, b \frac{dP_\alpha(\epsilon_k,b)}{d\epsilon_k} , \tag{30}$$

where we have solved the time-dependent equations for a series of impact parameters b, and n_α is the occupation number for Hartree-Fock single-particle state α. The theoretical differential cross section peaks around 8 MeV and decays exponentially at higher energies as observed in the experiment.[18] The curve can be approximated by a function of the form $K\sqrt{\epsilon}e^{-\epsilon/T}$ with a temperature $T=4.8$ MeV and $K=250$. Other methods failed to reproduce any of these properties, resulting, for example, in either flat nucleon energy spectra or unphysical peaks.

V. SUMMARY

In summary, we have introduced a method for the calculation of excitation probabilities in external field problems represented by discretized Hamiltonians. The method is most suitable for large numerical problems in two and three dimensions where the storage of the full Hamiltonian matrix is not feasible. As a demonstration of the formalism we have computed the excitation probabilities for a model problem by solving the Schrödinger equation in spherical and in cylindrical coordinates, using the numerical formalism described in this paper. As a realistic problem we have studied the prompt nucleon emission in low energy heavy-ion collisions. We believe that the utilization of the method will significantly improve our ability to extract dynamical information from a large class of nuclear, atomic, and quantum field-theoretic problems.

This research was sponsored in part by the U. S. Department of Energy under Contract No. DE-AC05-84OR21400 with Martin Marietta Energy Systems, Inc., and with Vanderbilt University under Contract No. DE-FG05-87ER40376.

APPENDIX A

In this appendix we will discuss the numerical methods employed for the solution of the time-dependent Schrödinger equation in cylindrical coordinates. In order to obtain discretized equations which satisfy the conservation laws, we use the variation after discretization method of Ref. 16.

Consider the energy functional

$$E\langle\psi\,|\,\psi\rangle=\langle\psi\,|\,H\,|\,\psi\rangle = \int d^3r\,\psi^*(\mathbf{r})\left[-\frac{\hbar^2}{2m}\nabla^2+V\right]\psi(\mathbf{r}) , \tag{A1}$$

where $\mathbf{r}=(r,\phi,z)$ denotes the cylindrical coordinates, and we have omitted the subscripts distinguishing the different eigenvectors and eigenvalues of the Hamiltonian. To generalize all of the equations below, just add subscripts to wave functions and energies. Equation (A1) can be written in a more symmetric fashion by performing an integration by parts

$$E\int dr\,dz\,r\,|\,\chi\,|^2=\int dr\,dz\,r\left[\frac{\hbar^2}{2m}\left(\left|\frac{\partial\chi}{\partial r}\right|^2+\left|\frac{\partial\chi}{\partial z}\right|^2\right)+\left[V+\frac{\hbar^2\mu^2}{2mr^2}\right]|\,\chi\,|^2\right] , \tag{A2}$$

where we have used the explicit form of the ∇ operator in cylindrical coordinates and the transformation

$$\psi(\mathbf{r})=\frac{e^{i\mu\phi}}{\sqrt{2\pi}}\chi(r,z) . \tag{A3}$$

The discretization of Eq. (A2) in spatial coordinates r and z is implemented by using the following mesh

$$r_j=(j-\tfrac{1}{2})\Delta r,\quad j=1,2,\ldots,N_r ,$$
$$z_k=(k-N_z/2)\Delta z,\quad k=1,\ldots,N_z , \tag{A4}$$

as follows

$$E\sum_{j=1}^{N_r}\sum_{k=1}^{N_z}\Delta r\Delta z r_j\,|\,\chi_{jk}\,|^2=\sum_{j=1}^{N_r}\sum_{k=1}^{N_z}\Delta r\Delta z r_j\left[\frac{\hbar^2}{2m}\left|\frac{\chi_{j+1,k}-\chi_{jk}}{\Delta r}\right|^2\frac{r_{j+1/2}}{r_j}+\frac{\hbar^2}{2m}\left|\frac{\chi_{j,k+1}-\chi_{jk}}{\Delta z}\right|^2+\left[V_{jk}+\frac{\hbar^2\mu^2}{2mr_j^2}\right]|\,\chi_{jk}\,|^2\right] , \tag{A5}$$

where the multiplicative factor $r_{j+1/2}/r_j$ in the first term is included because for this term the r in the integration weights should be evaluated at the midinterval point (due to the derivative in r), and we have defined $\chi_{jk}=\chi(r_j,z_k)$. In the next step we make the transformation

$$\chi_{jk}=\frac{g_{jk}}{\sqrt{r_j}}\ , \tag{A6}$$

to obtain

$$E\sum_{jk}\Delta r\Delta z\,|\,g_{jk}\,|^2=\sum_{jk}\Delta r\Delta z\left[\frac{\hbar^2}{2m(\Delta r)^2}\left|\frac{g_{j+1,k}}{\sqrt{r_{j+1}}}-\frac{g_{jk}}{\sqrt{r_j}}\right|^2 r_{j+1/2}+\frac{\hbar^2}{2m(\Delta z)^2}\,|\,g_{j,k+1}-g_{jk}\,|^2\right.$$
$$\left.+\left[V_{jk}+\frac{\hbar^2\mu^2}{2mr_j^2}\right]|\,g_{jk}\,|^2\right]\ . \tag{A7}$$

The normalization and boundary conditions are

$$\sum_{jk}\Delta r\Delta z\,|\,g_{jk}\,|^2=1,\quad g_{0k}=g_{N_r+1,k}=g_{j,0}=g_{j,N_z+1}=0\ .$$

The variation of Eq. (A7) with respect to $g^*_{j'k'}$ yields the eigenvalue equation

$$(\mathcal{H}g)_{jk}+(\mathcal{V}g)_{jk}=Eg_{jk}\ , \tag{A8}$$

where the quantities $\mathcal{H},\mathcal{V}$ denote the *horizontal* and *vertical* Hamiltonians, respectively, and they are defined by their action on g

$$(\mathcal{H}g)_{jk}=-\frac{\hbar^2}{2m(\Delta z)^2}(g_{j,k+1}+g_{j,k-1}-2g_{jk})+\frac{1}{2}\left[V_{jk}+\frac{\hbar^2\mu^2}{2mr_j^2}\right]g_{jk}\ ,$$
$$(\mathcal{V}g)_{jk}=-\frac{\hbar^2}{2m(\Delta r)^2}(C_jg_{j+1,k}+C_{j-1}g_{j-1,k}-2g_{jk})+\frac{1}{2}\left[V_{jk}+\frac{\hbar^2\mu^2}{2mr_j^2}\right]g_{jk}\ , \tag{A9}$$

with

$$C_j\equiv\frac{j}{\sqrt{j^2-1/4}}\ . \tag{A10}$$

To find the lowest energy eigenstate corresponding to the potential discussed in Sec. III, we use the *gradient iteration method* ($\mu=0$);

$$g^{n+1}=g^n-x_0D_rD_z[(\mathcal{H}g^n)+(\mathcal{V}g^n)-E^ng^n]\ , \tag{A11}$$

where the superscript n denotes the iteration index and E^n is the expectation value of the Hamiltonian evaluated using the nth-step wave functions. In Eq. (A11) the quantity x_0 is a small multiplicative constant and the *damping matrices* D_r and D_z are defined as

$$D_r=(1+T_r/E_0)^{-1}\ ,$$
$$D_z=(1+T_z/E_0)^{-1}\ ,$$

where T_r and T_z are the kinetic energy matrices in r and z directions, respectively, and E_0 determines the frequency cutoff scale for the damping procedure. The generalization of Eq. (A11) to more than one state can be achieved by adding a quantum label to the wave functions and energies. However, in this case the set of wave functions must be orthonormalized at each iteration. Further details of the *gradient iteration method* are given in Ref. 19. In practical calculations we have used $x_0=0.1$, and $E_0=10$ MeV. These values yield an energy convergence of 1 part of 10^{12} in approximately 150 static iterations.

Next, we solve the time-dependent Schrödinger equation

$$i\hbar\frac{\partial g(t)}{\partial t}=[\mathcal{H}'(t)+\mathcal{V}'(t)]g(t)\ , \tag{A12}$$

where the primes of $\mathcal{H}$ and $\mathcal{V}$ indicate the addition of time-dependent contributions $\frac{1}{2}W(t)$. The time-evolution operator over a small time interval Δt is approximated by the Peaceman-Rachford expression[16]

$$g(t_{n+1})=\left[1+\frac{\Delta t}{2\hbar}\mathcal{V}'\right]^{-1}\left[1-\frac{\Delta t}{2\hbar}\mathcal{H}'\right]\times\left[1+\frac{\Delta t}{2\hbar}\mathcal{H}'\right]^{-1}\left[1-\frac{\Delta t}{2\hbar}\mathcal{V}'\right]g(t_n)\ , \tag{A13}$$

where $t_n=(n-N_t/2)\Delta t$ is the discretized time. Note that this expression only requires the inversion of small matrices in r and z directions, and is accurate to order $(\Delta t)^2$.

[1] A. S. Umar, M. R. Strayer, D. J. Ernst, and K. R. S. Devi, Phys. Rev. C **30**, 1934 (1984), and references therein; A. S. Umar, M. R. Strayer, and D. J. Ernst, Phys. Lett. **140B**, 290 (1984); Phys. Rev. Lett. **55**, 584 (1985).

[2] N. Stolterfoht, Phys. Rep. **146**, 315 (1987).

[3] U. Heinz, W. Greiner, and B. Müller, Phys. Rev. A **23**, 562 (1981); D. Vasak, W. Greiner, B. Müller, T. Stahl, and M. Uhlig, Nucl. Phys. **A428**, 291 (1984).

[4] P. Pechukas, Phys. Rev. **181**, 174 (1969).

[5] P. Carruthers and F. Zachariason, Rev. Mod. Phys. **55**, 245 (1983).

[6] C. Bottcher and M. R. Strayer, Ann. Phys. **175**, 64 (1987).

[7] D. J. Ernst and M. R. Strayer, J. Phys. G (to be published).

[8] M. Tohyama, R. Kaps, D. Vasak, and U. Mosel, Nucl. Phys. **A437**, 739 (1985).

[9] M. L. Goldberger and K. M. Watson, *Collision Theory*

(Krieger, New York, 1975), p. 197.
[10]A. M. Lane and R. G. Thomas, Rev. Mod. Phys. **30**, 257 (1958).
[11]D. J. Ernst, C. M. Shakin, and R. M. Thaler, Phys. Rev. C **8**, 46 (1973).
[12]W. H. Bassichis and M. R. Strayer, Phys. Rev. C **20**, 915 (1979).
[13]J. T. Broad, Phys. Rev. A **18**, 1012 (1978).
[14]P. Bonche, S. E. Koonin, and J. W. Negele, Phys. Rev. C **13**, 1226 (1976).
[15]P. W. Langhoff, J. Sims, and C. T. Corcoran, Phys. Rev. A **10**, 829 (1974); P. W. Langhoff in *Electron Molecule and Photon Molecule Collisions,* edited by T. Rescigno, V. McKoy, and B. Schneider (Plenum, New York, 1979).
[16]K. T. R. Davies and S. E. Koonin, Phys. Rev. C **23**, 2042 (1981).
[17]G. R. Satchler and W. G. Love, Phys. Rep. **55**, 183 (1979).
[18]A. Gavron, R. L. Ferguson, F. E. Obenshain, F. Plasil, G. R. Young, D. G. Sarantites, and C. F. Maguire, Phys. Rev. Lett. **46**, 8 (1981).
[19]A. S. Umar, M. R. Strayer, R. Y. Cusson, P.-G. Reinhard, and D. A. Bromley, Phys. Rev. C **32**, 172 (1985).